Danfoss: Scroll Optimization

JENS GRAVESEN, CHRISTIAN HENRIKSEN,
AND PETER HOWELL

1 Introduction

The scroll compressor consists of two plane spiral/helix running inside each other, traditionally both scrolls are the same circle involute with constant wall thickness, see figure 1.

When the moving scroll follows a circular orbit the chambers moves inwards and the air or fluid trapped in the chambers is compressed. In the standard circle involute scroll compressor the volume of the compression chambers grows linearly when we move outwards and the compression rate of such a compressor is sufficient for air-condition, but not for freezers or refrigerators. One could try to increase the compression rate by having more chambers, but that would increase the leakage too.

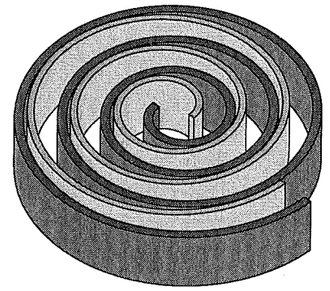

Figure 1: The standard circle involute scroll compressor.

The task from DANFOSS was to investigate how a change in the basic geometry of the scrolls and the orbit influence the compressor performance and efficiency, and then try to optimize the design.

We have not done any optimization, but we believe we have found a sound foundation for the optimization process. We can represent the geometry of the problem in a way which leads to closed expressions for all the geometric quantities which are interesting for the scroll design.

We have also analyzed the leakage between the compression chambers, and using a compressible lubrication model we have determined an expression which, appart from one integration, leads to a closed expression for the leakage.

2 The Geometry of Plane Curves

To fix the notation and terminology we give a brief introduction to the geometry of plane curves.

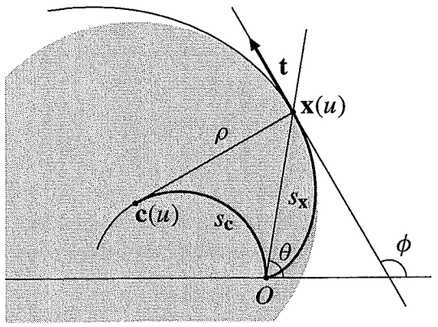

Figure 2: Some geometric concepts.

A parametrization of a regular plane curve is a differential map $\mathbf{x} : I \to \mathbb{R}^2$, such that $\mathbf{x}'(u) \neq \mathbf{0}$ all $u \in I$. The *unit tangent vector* is $\mathbf{t} = \frac{\mathbf{x}'}{|\mathbf{x}'|}$, the *unit normal vector* is $\mathbf{n} = \widehat{\mathbf{t}}$, and the *arc length* is given by $s = \int_0^u |\mathbf{x}'(t)|\, dt$.

We introduce the frame $(\mathbf{e}, \mathbf{f})$, given by $\mathbf{e}(u) = (\cos u, \sin u)$ and $\mathbf{f}(u) = (-\sin u, \cos u)$. The *tangent direction* ϕ is then given by $\mathbf{t} = \mathbf{e}(\phi)$, the *curvature* is $\kappa = \frac{d\phi}{ds}$ and the *radius of curvature* is $\rho = \frac{1}{\kappa} = \frac{ds}{d\phi}$. The *Frenet formulae* tells that $\frac{d\mathbf{t}}{ds} = \kappa\mathbf{n}$, $\frac{d\mathbf{n}}{ds} = -\kappa\mathbf{t}$, and hence $\mathbf{t}'(u) = s'(u)\frac{d\mathbf{t}}{ds} = s'(u)\kappa(u)\mathbf{n}(u)$ and likewise $\mathbf{n}'(u) = -s'(u)\kappa(u)\mathbf{t}(u)$. The *centre of curvature* is given by $\mathbf{c} = \mathbf{x} + \rho\mathbf{n}$. The *osculating circle* is the unique circle which has second order contact with the curve in the point $\mathbf{x}$, and it has centre $\mathbf{c}$ and radius ρ. The *evolute* is the the curve traced out by the centre of curvature:

$$\mathbf{c} = \mathbf{x} + \rho_{\mathbf{x}}\mathbf{n}_{\mathbf{x}}, \tag{1}$$

by differentiation we have

$$\mathbf{c}' = \mathbf{x}' + \rho'_{\mathbf{x}}\mathbf{n}_{\mathbf{x}} + \rho_{\mathbf{x}}\mathbf{n}'_{\mathbf{x}} = s'_{\mathbf{x}}\mathbf{t}_{\mathbf{x}} + \rho'_{\mathbf{x}}\mathbf{n}_{\mathbf{x}} - \rho_{\mathbf{x}}s'_{\mathbf{x}}\kappa_{\mathbf{x}}\mathbf{t}_{\mathbf{x}} = \rho'_{\mathbf{x}}\mathbf{n}_{\mathbf{x}}, \tag{2}$$

from which we see that if $\rho'_{\mathbf{x}} > 0$, then $\mathbf{c}$ is a regular curve, $\mathbf{t}_{\mathbf{c}} = \mathbf{n}_{\mathbf{x}}$, $s'_{\mathbf{c}} = \rho'_{\mathbf{x}}$, and hence $s_{\mathbf{c}} = \rho_{\mathbf{x}} + \text{constant}$. If $\rho'_{\mathbf{x}} \neq 0$ we can always obtain $\rho'_{\mathbf{x}} > 0$ by choosing the appropriate orientation. We can obviously invert this process and thus obtain $\mathbf{x}$ as an *involute* of the curve $\mathbf{c}$:

$$\mathbf{x} = \mathbf{c} - (s_{\mathbf{c}} + s_0)\mathbf{t}_{\mathbf{c}}, \tag{3}$$

and if $\mathbf{c}$ is a regular curve then $\rho_{\mathbf{x}}$ is a strictly increasing function. The following well known result tells us that an involute is a spiral:

Lemma 1. *Let $\mathbf{x}(u)$ be a regular curve with radius of curvature $\rho(u)$ and regular evolute $\mathbf{c}(u)$. Let $D(u)$ be the disk bounded by the osculating circle:*

$$D(u) = \{\mathbf{x} \in \mathbb{R}^2 \mid |\mathbf{x} - \mathbf{c}(u)| < \rho(u)\}.$$

If the radius of curvature $\rho(u)$ is a strictly increasing function, then the disks $D(u)$ forms an increasing nested sequence:

$$u_1 < u_2 \Rightarrow \overline{D(u_1)} \subset D(u_2), \tag{4}$$

and the past and future of the curve is respectively inside and outside the disk:

$$u_1 < u_2 \Rightarrow \mathbf{x}(u_1) \in D(u_2) \wedge \mathbf{x}(u_2) \notin D(u_1). \tag{5}$$

Furthermore, choose origo $O \in \bigcap_{t\in I} \overline{D(u)}$ and let (r, θ) be polar coordinates for the curve $\mathbf{x}$, then θ is an increasing function:

$$\theta'(u) > 0. \tag{6}$$

Proof. As $\mathbf{x}(u)$ is on the boundary of $D(u)$ (4) implies (5). Now let $\mathbf{x} \in D(u_1)$, then $|\mathbf{x} - \mathbf{c}(u_1)| \leq \rho(u_1)$, Furthermore $\mathbf{c}(u_1)$ and $\mathbf{c}(u_2)$ are points on the evolute and hence $|\mathbf{c}(u_2) - \mathbf{c}(u_1)| < s_{\mathbf{c}}(u_2) - s_{\mathbf{c}}(u_1) = \rho(u_2) - \rho(u_1)$. All in all we have:

$$\begin{aligned}|\mathbf{x} - \mathbf{c}(u_2)| &\leq |\mathbf{x} - \mathbf{c}(u_1)| + |\mathbf{c}(u_2) - \mathbf{c}(u_1)| \\ &< \rho(u_1) + \rho(u_2) - \rho(u_1) = \rho(u_2),\end{aligned}$$

which proves (4) and hence (5).

The angle between the line from $\mathbf{c}(u)$ to $\mathbf{x}(u)$ and the tangent $\mathbf{t}(u)$ is $\frac{\pi}{2}$, but then the angle between a line from any point in $D(u)$ to $\mathbf{x}(u)$ and the tangent is in the interval $(0, \pi)$. Because of (4) this is in particular true for the point O, and then (6) holds. □

We will later consider an orbiting curve so let us now consider a family of curves $\mathbf{x}_t(u) = \mathbf{X}(u, t)$. An *envelope* of such a family is a curve $\mathbf{y}$ which is tangential to the curve $\mathbf{x}_t$ at the point $\mathbf{y}(t)$. That means there exists a function $\mathbf{u}(t)$ such that

$$\mathbf{y}(t) = \mathbf{X}(u(t), t), \tag{7}$$

the derivative is then $\mathbf{y}'(t) = u'(t)\frac{\partial \mathbf{X}}{\partial u}(u(t), t) + \frac{\partial \mathbf{X}}{\partial t}(u(t), t)$. The derivative of $\mathbf{x}_t$ at the same point is $\mathbf{x}'_t(u(t)) = \frac{\partial \mathbf{X}}{\partial u}(u(t), t)$, so $\mathbf{y}'(t)$ and $\mathbf{x}'_t(u(t))$ are parallel if and only if

$$\left[\frac{\partial \mathbf{X}}{\partial t}(u(t), t)\, \frac{\partial \mathbf{X}}{\partial u}(u(t), t)\right] = 0, \tag{8}$$

where $[\mathbf{u}\,\mathbf{v}] = \widehat{\mathbf{u}} \cdot \mathbf{v}$ denotes the planar product, or determinant, of two vectors $\mathbf{u}$ and $\mathbf{v}$. Equation (8) determines the function $u(t)$ which then inserted in (7) gives the envelope $\mathbf{y}(t)$, see figure 3.

3 Scroll Geometry

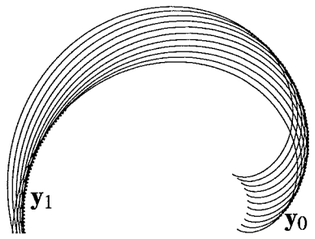

Figure 3: Two envelopes.

Suppose the curve $\mathbf{x}$ describes one side of a moving scroll wall. The side of the moving wall can be described by

$$\mathbf{X}(u,t) = \mathbf{R}\big(\psi(t)\big)\big(\mathbf{x}(u) + \mathbf{a}(t)\big),$$

where $\mathbf{a}$ denotes the translation and $\mathbf{R}(\psi)$ denotes rotation by the angle ψ. The mating side $\mathbf{y}$ of the fixed scroll wall is given by the envelope of the family of curves $\mathbf{X}$, and consequently satisfies (7) and (8). In general (8) is an unpleasant nonlinear equation, but if we use the *tangent direction* as the parameter on both curves, i.e., $u = \phi_{\mathbf{x}}$ and $t = \phi_{\mathbf{y}}$, then the equations are simplified to

$$t = u + \psi(t) + n\pi, \quad n \in \mathbb{Z}, \tag{9}$$

$$\mathbf{y}_n(t) = \mathbf{R}\big(\psi(t)\big)\big(\mathbf{x}\big(t - \psi(t) - n\pi\big) + \mathbf{a}(t)\big) \tag{10}$$

If $\mathbf{a}$ and ψ are periodic with period 2π, then we have $\mathbf{y}_n(t + 2\pi) = \mathbf{y}_{n+2}(t)$ and we have only two candidates for the mating side of the fixed scroll wall:

$$\mathbf{y}_0(t) = \mathbf{R}\big(\psi(t)\big)\big(\mathbf{x}\big(t - \psi(t)\big) + \mathbf{a}(t)\big),$$
$$\mathbf{y}_1(t) = \mathbf{R}\big(\psi(t)\big)\big(\mathbf{x}\big(t - \psi(t) - \pi\big) + \mathbf{a}(t)\big).$$

We may reparameterize $\mathbf{y}_1$, by $t \mapsto t + \pi$, and can then write

$$\mathbf{y}_i(t) = \mathbf{R}\big(\psi_i(t)\big)\big(\mathbf{x}\big(t - \psi_i(t)\big) + \mathbf{a}_i(t)\big), \quad i = 0, 1, \tag{11}$$

where $\mathbf{a}_i$ and ψ_i are defined by

$$\mathbf{a}_i(t) = \begin{cases} \mathbf{a}(t) & \text{if } i = 0, \\ \mathbf{a}(t+\pi) & \text{if } i = 1. \end{cases} \qquad \psi_i(t) = \begin{cases} \psi(t) & \text{if } i = 0, \\ \psi(t+\pi) & \text{if } i = 1. \end{cases} \tag{12}$$

At time t the side $\mathbf{x}_t$ of the moving scroll wall and mating side $\mathbf{y}_0$ of the fixed scroll wall touch each other in a series of points:

$$\mathbf{y}_0(t + 2n\pi) = \mathbf{R}\big(\psi(t)\big)\big(\mathbf{x}\big(t + 2n\pi - \psi(t)\big) + \mathbf{a}(t)\big), \tag{13}$$

and at time $t + \pi$, the curves $\mathbf{x}_{t+\pi}$ and $\mathbf{y}_1$ touch in the points:

$$\mathbf{y}_1(t + 2n\pi) = \mathbf{R}\big(\psi(t+\pi)\big)\big(\mathbf{x}\big(t + 2n\pi - \psi(t+\pi)\big) + \mathbf{a}(t+\pi)\big), \tag{14}$$

and between these points the two walls bounds a chamber, (the compression chamber of the scroll compressor), see figure 4.

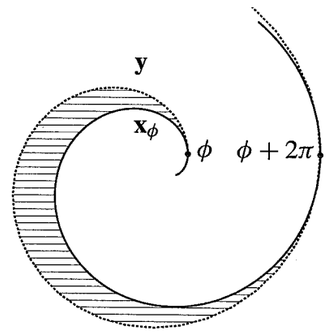

Figure 4: A compression chamber.

Excluding rotation

If we exclude rotation, i.e., let $\psi = 0$, then we just have

$$\mathbf{y}_0(t) = \mathbf{x}(t) + \mathbf{a}(t),$$
$$\mathbf{y}_1(t) = \mathbf{x}(t) + \mathbf{a}(t + \pi).$$

Circular orbit

If $\mathbf{a}$ is a circle with centre O, with radius R, and parametrized by tangent direction, then $\mathbf{a} = -R\mathbf{f}$, and we have

Lemma 2. *Let $\mathbf{x}$ be a regular curve, and put $\mathbf{X}(u,t) = \mathbf{x}_t(u) = \mathbf{x}(u) - R\mathbf{f}(t)$. The envelopes of this family are $\mathbf{y} = \mathbf{x} \mp R\mathbf{f}$, and they have the same evolute as $\mathbf{x}$.*

Proof. Let $\mathbf{c} = \mathbf{x} + \rho_{\mathbf{x}}\mathbf{n}_{\mathbf{x}}$ be the evolute of $\mathbf{x}$. If we parametrize $\mathbf{x}$ by tangent direction, then we have $\mathbf{x} = \mathbf{c} - (s_{\mathbf{c}} + s_0)\mathbf{t}_{\mathbf{c}} = \mathbf{c} - (s_{\mathbf{c}} + s_0)\mathbf{n}_{\mathbf{x}} = \mathbf{c} - (s_{\mathbf{c}} + s_0)\mathbf{f}$, but then $\mathbf{y} = \mathbf{x} \mp R\mathbf{f} = \mathbf{c} - (s_{\mathbf{c}} + (s_0 \pm R))\mathbf{f} = \mathbf{c} - (s_{\mathbf{c}} + (s_0 \pm R))\mathbf{t}_{\mathbf{c}}$, and we see that $\mathbf{y}$ is an involute of $\mathbf{c}$ too. □

3.1 Using the natural equation

If the side $\mathbf{x}$ of the moving scroll wall is given by some parametrization, then it is in general impossible to find the parametrization by tangents direction. Instead we will specify the curve by the *natural equation* in the form $s = s(\phi)$ where s denotes arc-length on the curve and ϕ denotes the tangent direction of the curve. If s is a positive, increasing and convex function, then $\rho' = s'' > 0$ and by Lemma 1 the corresponding curve is a spiral.

The *tangent vector* $\mathbf{t}(\phi)$ of $\mathbf{x}(\phi)$ is by definition of ϕ the vector $\mathbf{e}(\phi)$, and hence

$$\mathbf{x}' = \frac{ds_{\mathbf{x}}}{d\phi}\mathbf{t} = s'_{\mathbf{x}}\mathbf{e} \tag{15}$$

and

$$\mathbf{x} = \int s'_{\mathbf{x}}\mathbf{e}\,d\phi = s_{\mathbf{x}}\mathbf{e} - \int s_{\mathbf{x}}\mathbf{f}\,d\phi. \tag{16}$$

Observe that we can find an *explicit* expression for the parametrization of $\mathbf{x}$ if we can integrate $s(\phi)\cos(\phi)$ analytically, this is for example the case if s is a polynomial or a piecewise polynomial in ϕ. The mating sides of the fixed scroll walls are given by

$$\mathbf{y}_i(\phi) = \mathbf{R}\big(\psi_i(\phi)\big)\mathbf{x}\big(\phi - \psi_i(\phi)\big) + \mathbf{a}_i(\phi), \quad i = 0, 1. \tag{17}$$

Excluding rotation

If we exclude the rotation, then we get particularly simple equations

$$\mathbf{y}_0(\phi) = \mathbf{x}(\phi) + \mathbf{a}(\phi), \qquad \mathbf{y}_1(\phi) = \mathbf{x}(\phi) + \mathbf{a}(\phi + \pi), \tag{18}$$

$$\mathbf{y}_0'(\phi) = \big(s_{\mathbf{x}}'(\phi) + s_{\mathbf{a}}'(\phi)\big)\mathbf{e}(\phi), \qquad \mathbf{y}_1'(\phi) = \big(s_{\mathbf{x}}'(\phi) - s_{\mathbf{a}}'(\phi + \pi)\big)\mathbf{e}(\phi), \tag{19}$$

$$s_{\mathbf{y}_0}(\phi) = s_{\mathbf{x}}(\phi) + s_{\mathbf{a}}(\phi), \qquad s_{\mathbf{y}_1}(\phi) = s_{\mathbf{x}}(\phi) - s_{\mathbf{a}}(\phi + \pi), \tag{20}$$

$$\rho_{\mathbf{y}_0}(\phi) = \rho_{\mathbf{x}}(\phi) + \rho_{\mathbf{a}}(\phi), \qquad \rho_{\mathbf{y}_1}(\phi) = \rho_{\mathbf{x}}(\phi) - \rho_{\mathbf{a}}(\phi + \pi), \tag{21}$$

where ρ denotes the radius of curvature. If we assume that $\rho_{\mathbf{x}}, \rho_{\mathbf{a}} > 0$, (which we always can do by picking the right orientation) then (21) implies that $\mathbf{y}_0$ is on the 'outside' of $\mathbf{x}$ and $\mathbf{y}_1$ is on the 'inside' of $\mathbf{x}$, see figure 3.

3.2 The natural equation for a closed plane curve

Let $s_{\mathbf{a}} = s_{\mathbf{a}}(\phi)$ be the natural equation for the closed curve $\mathbf{a}$. It is clear that we must have $s_{\mathbf{a}}(\phi + 2\pi) - s_{\mathbf{a}}(\phi) = 2\pi R$, where $2\pi R$ is the length of the closed curve. It is therefore natural to put

$$s_{\mathbf{a}}(\phi) = \bar{s}_{\mathbf{a}}(\phi) + R\phi \tag{22}$$

where $\bar{s}_{\mathbf{a}}$ is a periodic function of ϕ with period 2π. As $\mathbf{a} = s_{\mathbf{a}}\mathbf{e} - \int s_{\mathbf{a}}\mathbf{f}\,d\phi$ we see that $\mathbf{a}$ is closed if and only if $\big(s_{\mathbf{a}}(2\pi) - s_{\mathbf{a}}(0)\big)\mathbf{e}(0) - \int_0^{2\pi} s_{\mathbf{a}}\mathbf{f}\,d\phi = \mathbf{0}$. Inserting (22) we get the equation $\int_0^{2\pi} \bar{s}_{\mathbf{a}}\mathbf{f}\,d\phi = \mathbf{0}$ or the two scalar equations

$$\int_0^{2\pi} \bar{s}_{\mathbf{a}}(\phi)\cos(\phi)\,d\phi = 0, \qquad \int_0^{2\pi} \bar{s}_{\mathbf{a}}(\phi)\sin(\phi)\,d\phi = 0. \tag{23}$$

That is, the Fourier expansion of $\bar{s}_{\mathbf{a}}$ is

$$\bar{s}_{\mathbf{a}}(\phi) = \sum_{n=2}^{\infty}\big(a_n\cos(n\phi) + b_n\sin(n\phi)\big). \tag{24}$$

Using only a finite trigonometric polynomial of this kind we can get a closed expression for the curve $\mathbf{a}$ parametrized by tangent direction. We finally note that the case $\bar{s}_{\mathbf{a}} = 0$ corresponds to that of a circle with radius R, $\mathbf{a} = -R\mathbf{f}$.

3.3 The volume of the compression chambers

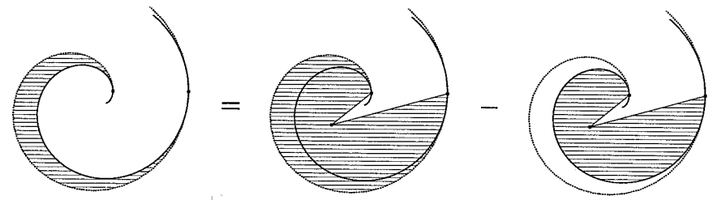

Figure 5: The volume of a compression chamber.

A compression chamber is bounded by two curve segments, so we can find the volume of the chamber as the difference between the areas spanned by a fixed point and the two curve segments, see figure 5.

When we want to find the area spanned by a point and a segment of a curve, then we first observe that the area of the triangle spanned by $\mathbf{r}$ and $\mathbf{r}'$ is $\frac{1}{2}[\mathbf{r}\,\mathbf{r}']$, so the area spanned by O and the segment of the curve $\mathbf{r}$ is given by $\text{Area} = \frac{1}{2}\int_{t_1}^{t_2}[\mathbf{r}\,\mathbf{r}']\,dt$, see figure 6, this is also a consequence of Green's theorem. Observe that a rotation around O does not change the area. So up to a sign the volume of a chamber in the scroll compressor is given by

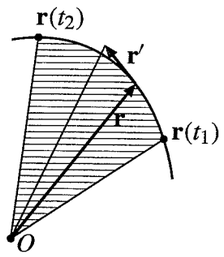

Figure 6: The area spanned by a point and a curve.

$$\begin{aligned} v_i(\phi) &= \frac{1}{2}\int_{\phi}^{\phi+2\pi}[\mathbf{y}_i(t)\,\mathbf{y}_i'(t)]\,dt - \frac{1}{2}\int_{\phi-\psi_i(\phi)}^{\phi-\psi_i(\phi)+2\pi}\big[\big(\mathbf{x}(t) + \mathbf{a}_i(\phi)\big)\,\mathbf{x}'(t)\big]\,dt \\ &= \frac{1}{2}\int_{\phi}^{\phi+2\pi}[\mathbf{y}_i(t)\,\mathbf{y}_i'(t)]\,dt - \frac{1}{2}\int_{\phi-\psi_i(\phi)}^{\phi-\psi_i(\phi)+2\pi}[\mathbf{x}(t)\,\mathbf{x}'(t)]\,dt \\ &\quad - \frac{1}{2}\big[\mathbf{a}_i(\phi)\,\big(\mathbf{x}\big(\phi - \psi_i(\phi) + 2\pi\big) - \mathbf{x}\big(\phi - \psi_i(\phi)\big)\big)\big]. \end{aligned} \tag{25}$$

Excluding rotation

Without rotation we have

$$\begin{aligned} v_i(\phi) = \frac{1}{2}\int_{\phi}^{\phi+2\pi}&\big([\mathbf{y}_i(t)\,\mathbf{y}_i'(t)] - [\mathbf{x}(t)\,\mathbf{x}'(t)]\big)\,dt \\ &- \frac{1}{2}\big[\mathbf{a}_i(\phi)\,\big(\mathbf{x}(\phi + 2\pi) - \mathbf{x}(\phi)\big)\big]. \end{aligned} \tag{26}$$

Once more we have that if $s_{\mathbf{x}}(\phi)$ is a piecewise polynomial and $\overline{s}_{\mathbf{a}}(\phi)$ is a finite trigonometric polynomial, then we have $v_i(\phi)$ on closed form.

3.4 Circular orbit

If we specialize to the case of a circular orbit $\mathbf{a} = -R\mathbf{f}$, and no rotation, then $\mathbf{a}_0 = \mathbf{a}$ and $\mathbf{a}_1 = -\mathbf{a}$ and hence

$$\mathbf{y}(t) = \mathbf{x}(t) \mp R\mathbf{f}(t), \tag{27}$$

$$\mathbf{y}'(t) = \mathbf{x}'(t) \pm R\mathbf{e}(t), \tag{28}$$

$$\begin{aligned}
[\mathbf{y}(t)\,\mathbf{y}'(t)] &= [\mathbf{x}(t)\,\mathbf{x}'(t)] \pm R[\mathbf{x}(t)\,\mathbf{e}(t)] \mp R[\mathbf{f}(t)\,\mathbf{x}'(t)] - R^2[\mathbf{f}(t)\,\mathbf{e}(t)] \\
&= [\mathbf{x}(t)\,\mathbf{x}'(t)] \pm R\Big(\frac{d}{dt}[\mathbf{x}(t) - \mathbf{f}(t)] - [\mathbf{x}'(t) - \mathbf{f}(t)]\Big) \\
&\quad \pm R[\mathbf{x}'(t)\,\mathbf{f}(t)] + R^2 \\
&= [\mathbf{x}(t)\,\mathbf{x}'(t)] \pm R\frac{d}{dt}[\mathbf{x}(t) - \mathbf{f}(t)] \pm 2R[\mathbf{x}'(t)\,\mathbf{f}(t)] + R^2 \\
&= [\mathbf{x}(t)\,\mathbf{x}'(t)] \pm \frac{d}{dt}R[\mathbf{f}(t)\,\mathbf{x}(t)] \pm 2Rs'_{\mathbf{x}}(t) + R^2
\end{aligned}$$

$$\rho_{\mathbf{y}} = \rho_{\mathbf{x}} \pm R \tag{29}$$

$$s_{\mathbf{y}} = s_{\mathbf{x}} + \begin{cases} R\phi \\ -R(\phi + \pi) \end{cases} \tag{30}$$

The volume of a compression chamber is given by

$$\begin{aligned}
v(\phi) &= \frac{1}{2}\int_{\phi}^{\phi+2\pi} \big([\mathbf{y}(t)\,\mathbf{y}'(t)] - [\mathbf{x}(t)\,\mathbf{x}'(t)]\big)\,dt \\
&\quad \mp \frac{1}{2}\big[\mathbf{a}(\phi)\,\big(\mathbf{x}(\phi+2\pi) - \mathbf{x}(\phi)\big)\big] \\
&= \pm\frac{1}{2}\int_{\phi}^{\phi+2\pi} \left(\frac{d}{dt}R[\mathbf{f}(t)\,\mathbf{x}(t)] + 2Rs'_{\mathbf{x}}(t) \pm R^2\right) dt \\
&\quad \pm \frac{1}{2}R\big[\mathbf{f}(\phi)\,\big(\mathbf{x}(\phi+2\pi) - \mathbf{x}(\phi)\big)\big] \\
&= \pm\frac{1}{2}\Big(R[\mathbf{f}(\phi+2\pi)\,\mathbf{x}(\phi+2\pi)] - R[\mathbf{f}(\phi)\,\mathbf{x}(\phi)] \\
&\qquad + 2Rs_{\mathbf{x}}(\phi+2\pi) - 2Rs_{\mathbf{x}}(\phi) \pm 2\pi R^2 \\
&\qquad + R\big[\mathbf{f}(\phi)\,\big(\mathbf{x}(\phi+2\pi) - \mathbf{x}(\phi)\big)\big]\Big) \\
&= \pi R^2 \pm R\Big(\big[\mathbf{f}(\phi)\,\big(\mathbf{x}(\phi+2\pi) - \mathbf{x}(\phi)\big)\big] + s_{\mathbf{x}}(\phi+2\pi) - s_{\mathbf{x}}(\phi)\Big)
\end{aligned} \tag{31}$$

3.5 The other side of the wall

So far we have only considered one pair of mating sides of the scroll walls, but in a real world scroll compressor we have of course two pairs of mating sides. In this section we will address the problem of defining both sides of the scroll wall.

Constant wall thickness

It seems natural to try to make walls of constant thickness as in the case of the standard circle involute scroll scroll compressor, see figure 1.

Let the curve describing one side of the moving scroll wall be $\mathbf{x}(\phi)$, with the natural equation $s = s_{\mathbf{x}}(\phi)$. We can write $\mathbf{x} = \mathbf{c} - (s_{\mathbf{c}} + s_0)\mathbf{t}_{\mathbf{c}}$, where $\mathbf{c}$ is the evolute of $\mathbf{x}$. Any curve $\widetilde{\mathbf{x}}$ parallel to $\mathbf{x}$ is also an involute of $\mathbf{c}$, thus

$$\widetilde{\mathbf{x}} = \mathbf{c} - (s_{\mathbf{c}} + s_1)\mathbf{t}_{\mathbf{c}} = \mathbf{x} - w\mathbf{n}_{\mathbf{x}} = \mathbf{x} - w\mathbf{f}, \tag{32}$$

where $w = s_1 - s_0$ is the distance between the curves. The thickness w has a sign and if $w > 0$, then the parallel curve $\widetilde{\mathbf{x}}$ is on the 'outside' of $\mathbf{x}$. The curvatures are related by the equation $\rho_{\widetilde{\mathbf{x}}} = \rho_{\mathbf{x}} + w$, and as $\rho = \frac{ds}{d\phi}$, the natural equation $s = s_{\widetilde{\mathbf{x}}}(\phi)$ of $\widetilde{\mathbf{x}}$ is given by $s_{\widetilde{\mathbf{x}}}(\phi) = s_{\mathbf{x}}(\phi) + w\phi$. Observe that it is only in the case of parallel curves we have such nice relations. If we put $\widetilde{\mathbf{x}}(t) = \mathbf{x}(t) + w(t)\mathbf{n}_{\mathbf{x}}(t)$ with $w(t)$ a non constant function, then $\phi_{\widetilde{\mathbf{x}}} \neq \phi_{\mathbf{x}}$, and we have do not have any explicit formula linking the curvature of $\mathbf{x}$ and $\widetilde{\mathbf{x}}$.

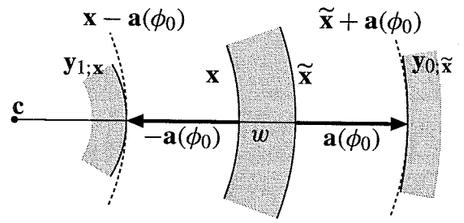

Figure 7: A scroll compressor with a moving scroll of constant width.

We now let the wall follow the orbit of $\mathbf{a}$, and restrict ourself to the case of a circular orbit, $\mathbf{a} = -R\mathbf{f}$, and with constant width $w > 0$. In that case we have a situation as in figure 7, where we see the moving scroll wall bounded by $\mathbf{x}$ and $\widetilde{\mathbf{x}}$ in the channel defined by the fixed scroll wall. By Lemma 2 we have that $\mathbf{y}_{1;\mathbf{x}}$ has the same evolute as $\mathbf{x}$ and $\mathbf{y}_{0;\widetilde{\mathbf{x}}}$ has the same evolute as $\widetilde{\mathbf{x}}$, in particular are $\mathbf{y}_{1;\mathbf{x}}$ and $\mathbf{y}_{0;\widetilde{\mathbf{x}}}$ parallel curves and we have the following result:

Lemma 3. *If a scroll wall of constant width w is moved in circular orbit with radius R, then the channel of the fixed scroll has constant width, $w + 2R$.*

The fixed scroll wall will in general *not* have constant thickness, the following result tells us when this happens:

Proposition 4. *Let $\mathbf{x}$ and $\widetilde{\mathbf{x}}$ be the sides of the moving scroll wall which moves in circular orbit and let $\mathbf{y} = \mathbf{y}_{1;\mathbf{x}}$ and $\widetilde{\mathbf{y}} = \mathbf{y}_{0;\widetilde{\mathbf{x}}}$ be the mating sides of the fixed scroll wall, as in figure 7.*

If the curves are spirals in the sense that the arclength of any of the curves is a strictly increasing convex function of the tangent direction, then the following statements are equivalent:

1. *The thickness of the scroll walls are constant.*
2. *The curves $\mathbf{x}$ and $\widetilde{\mathbf{x}}$ have a common simple closed convex evolute.*
3. *The curves $\mathbf{y}$ and $\widetilde{\mathbf{y}}$ have a common simple closed convex evolute.*
4. *The curves $\mathbf{x}$, $\widetilde{\mathbf{x}}$, $\mathbf{y}$, and $\widetilde{\mathbf{y}}$ have a common simple closed convex evolute.*

Proof. We will assume that all four curves are parametrized by tangent direction and that the circular orbit is given by $\mathbf{a} = -R\mathbf{f}$.

Assume that the wall thickness of the moving scroll wall is constant, then all four curves $\mathbf{x}$, $\widetilde{\mathbf{x}}$, $\mathbf{y}$, and $\widetilde{\mathbf{y}}$ are parallel curves by Lemma 3, and hence they have a common evolute $\mathbf{c}$. That $\mathbf{c}$ is convex, i. e., has nonvanishing curvature, follows from the fact that the scroll sides are smooth curves.

Suppose that the fixed scroll wall has constant thickness too, then the curve which together with $\widetilde{\mathbf{y}}$ defines the fixed scroll wall is of the form $\phi \mapsto \mathbf{y}(\phi + \nu)$. As the tangent direction is the same and the curves are spirals, we must have $\nu = 2\pi$. That means that the curve $\phi \mapsto \mathbf{y}(\phi + 2\pi)$ is parallel to $\widetilde{\mathbf{y}}$ and hence also to $\mathbf{y}$, but as parallel curves have common evolutes we must have that $\mathbf{c}(\phi) = \mathbf{c}(\phi + 2\pi)$ and the common evolute is closed. As $\phi + \frac{\pi}{2}$ is the tangent direction on the evolute we have that it is periodic with period 2π when parametrized by tangent direction, but then it can not have any self intersections and it must be a simple closed convex curve.

We have now shown that $1 \Rightarrow 4$, and we clearly have that $4 \Rightarrow 2, 3$. So we need only to show that $2 \Rightarrow 1$ and $3 \Rightarrow 1$. Now assume that $\mathbf{x}$ and $\widetilde{\mathbf{x}}$ are involutes of a common simple closed convex curve $\mathbf{c}$. By Lemma 3 we have that all four curves are parallel so we need only to show that $\mathbf{y}$ and the curve $\phi \mapsto \mathbf{y}(\phi + 2\pi)$ are parallel. As $\mathbf{y} = \mathbf{c} - (s_{\mathbf{c}} + s_0)\mathbf{f}$ we have that

$$\mathbf{y}(\phi + 2\pi) - \mathbf{y}(\phi) = -\big(s_{\mathbf{c}}(\phi + 2\pi) - s_{\mathbf{c}}(\phi)\big)\mathbf{f}(\phi) = -\ell_{\mathbf{c}}\mathbf{f}(\phi),$$

where $\ell_{\mathbf{c}}$ is the length of the closed curve $\mathbf{c}$. The tangent vector of both $\mathbf{y}(\phi + 2\pi)$ and $\mathbf{y}(\phi)$ are $\mathbf{e}$ which is orthogonal to $\mathbf{f}$, and we see that $\mathbf{y}(\phi + 2\pi)$ and $\mathbf{y}(\phi)$ indeed are parallel, and that the distance between them are $\ell_{\mathbf{c}}$.

To prove that $3 \Rightarrow 1$ we only have to interchange the role of the moving and fixed scroll wall. □

The lemma above gives us a way of constructing scroll compressors with constant wall thickness, unfortunately this does not give us much compared to the standard circle evolute scroll compressor. As $\mathbf{x}(\phi + 2\pi) - \mathbf{x}(\phi) = -\ell_{\mathbf{c}}\mathbf{f}(\phi)$, the expression (31) for the volume of a compression chamber reduces to

$$v(\phi) = \pi R^2 \pm R\big(s_{\mathbf{x}}(\phi + 2\pi) - s_{\mathbf{x}}(\phi)\big).$$

Furthermore if $\mathbf{c}$ is the closed evolute of $\mathbf{x}$, then $s'_{\mathbf{x}} = \rho_{\mathbf{x}} = s_{\mathbf{c}} + s_0$, so

$$\int_{\phi+2\pi}^{\phi+4\pi} s_{\mathbf{c}}(t)\,dt = \int_{\phi+2\pi}^{\phi+4\pi} \big(s_{\mathbf{c}}(t - 2\pi) + \ell_{\mathbf{c}}\big)\,dt = \int_{\phi}^{\phi+2\pi} s_{\mathbf{c}}(t)\,dt + 2\pi\ell_{\mathbf{c}}$$

and hence $v(\phi + 2\pi) - v(\phi) = 2\pi\ell_{\mathbf{c}}$. We see that only the size, not the shape of $\mathbf{c}$ matters, for the ratio between the volume of the chambers.

We can of course still have that only one of the scroll walls has constant width, but we would still have a problem. The volume function (31) for the two pairs of mating sides of the scroll walls will in general be different, and the compression rate would be different too.

Reflecting a pair of mating wall sides

The standard circle involute scroll compressor in figure 1 has the property that the two scroll walls are the image of each other by a reflection in a suitable point. By this reflection the two pairs of mating sides gets mapped into each other, see figure 8.

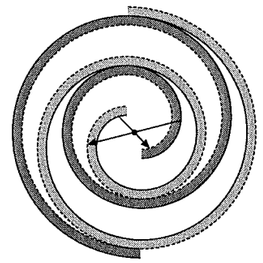

Figure 8: Reflection in a point.

We can convert this property to a principle by which we can construct the whole of the scroll walls once we have one pair $\mathbf{x}(\phi)$, $\mathbf{y}(\phi)$ of mating sides. In order to define the reflection which will give us the other pair of mating sides we need the centre of the reflection, and we only need the image of one point in order to determine the centre point.

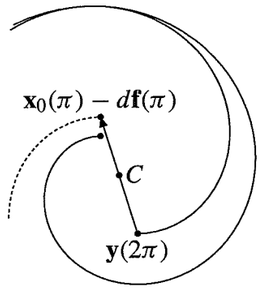

Figure 9: Reflecting a pair of mating sides in a point.

We are given one side $\mathbf{x}_t(\phi) = \mathbf{x}(\phi) - R\mathbf{f}(t)$ of the moving scroll and the mating side $\mathbf{y}(\phi) = \mathbf{x}_{\phi-\pi}(\phi)$ of the fixed scroll wall. We want the reflection to map the point $\mathbf{y}(2\pi)$ to the point $\mathbf{x}_0(\pi) - d\mathbf{f}(\pi)$ which we note lies on the normal to $\mathbf{x}_0$ opposite $\mathbf{y}$, see figure 9. The centre point C is determined by the equation $2C = \mathbf{y}(2\pi) + \mathbf{x}_0(\pi) - d\mathbf{f}(\pi)$, and then the other pair of mating scroll walls are determined by the equations $\widetilde{\mathbf{x}}_0(\phi) + \mathbf{y}(\phi + \pi) = 2C$ and $\widetilde{\mathbf{y}}(\phi) + \mathbf{x}_0(\phi - \pi) = 2C$, i.e.:

$$\widetilde{\mathbf{x}}(\phi) = \big(\mathbf{y}(2\pi) + \mathbf{x}(\pi) + (R-d)\mathbf{f}(\pi)\big) - \mathbf{y}(\phi + \pi) \tag{33}$$

$$\widetilde{\mathbf{y}}(\phi) = \big(\mathbf{y}(2\pi) + \mathbf{x}(\pi) + (R-d)\mathbf{f}(\pi)\big) - \mathbf{x}(\phi - \pi) \tag{34}$$

We have $\mathbf{y}(\phi) = \mathbf{x}_{\phi-\pi}(\phi) = \mathbf{x}(\phi) + R\mathbf{f}(\phi)$, and a short calculation shows that $\widetilde{\mathbf{y}}(\phi) = \widetilde{\mathbf{x}}_\phi(\phi - 2\pi)$. If $\mathbf{x}, \widetilde{\mathbf{x}} : [\pi, 2N\pi] \to \mathbb{R}^2$ and $\mathbf{y}, \widetilde{\mathbf{y}} : [2\pi, 2N + 2\pi] \to \mathbb{R}^2$, then at time $t \in [0, 2\pi)$ we see that the curves $\mathbf{x}_t$ and $\mathbf{y}$ touch each other in the points

$$\mathbf{y}(t + 2n\pi) = \mathbf{x}(t + 2n\pi) + R\mathbf{f}(t), \quad \begin{cases} n = 1, 2, \ldots, N & \text{if } t = 0, \\ n = 1, 2, \ldots, N-1 & \text{if } t \neq 0, \end{cases}$$

and the curves $\widetilde{\mathbf{x}}_t$ and $\widetilde{\mathbf{y}}$ touch each other in the points

$$\widetilde{\mathbf{y}}(t + 2n\pi) = \widetilde{\mathbf{x}}(t + 2n\pi - 2\pi) + R\mathbf{f}(t), \quad \begin{cases} n = 1, 2, \ldots, N & \text{if } t = \pi, \\ n = 2, 3, \ldots, N & \text{if } t \neq \pi. \end{cases}$$

Remember that the two pair of mating curves $\mathbf{x}$, $\mathbf{y}$ and $\widetilde{\mathbf{x}}$, $\widetilde{\mathbf{y}}$ are the reflected images of eachother and under this reflection we have the correspondens $\mathbf{x}(t + 2n\pi) \leftrightarrow \widetilde{\mathbf{y}}(t + (2n+1)\pi)$ and $\widetilde{\mathbf{x}}(t + (2n-1)\pi) \leftrightarrow \mathbf{y}(t + 2n\pi)$. This means that the sequence of chambers between $\mathbf{x}_t$ and $\mathbf{y}$ at time t is the same as the sequence of chambers between $\widetilde{\mathbf{x}}_{t+\pi}$ and $\widetilde{\mathbf{y}}$ at time $t + \pi$, we have in particular that the two 'channels' of the compressor have the same compression rate, which obviously is a desirable property.

3.6 Examples

We have considered three different natural equations: $s = \phi^2$ which gives the circle involute, and two others, $s = \phi^2 + \frac{1}{30}\phi^3$ and $s = \phi^2 - \frac{1}{50}\phi^3 + \frac{1}{400}\phi^4$. In

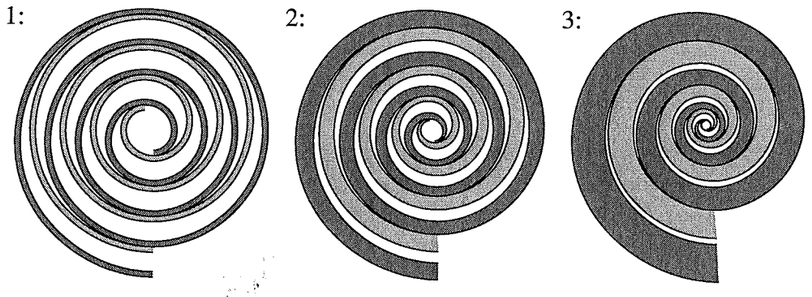

Figure 10: The three examples of scroll compressors.

all three cases we let $\mathbf{x}, \widetilde{\mathbf{x}} : [\pi, 8\pi] \to \mathbb{R}^2$ and $\mathbf{y}, \widetilde{\mathbf{y}} : [\pi, 10\pi] \to \mathbb{R}^2$ such that we at time $t = 2n\pi$, $n \in \mathbb{Z}$ have three chambers, with volume $v(2\pi)$, $v(4\pi)$, and $v(6\pi)$, where v is given by (31). We are interested in the ratio of these volumes so we have calculated $\Delta_1 = v(6\pi)/v(4\pi)$, $\Delta_2 = v(4\pi)/v(2\pi)$, and the overall volume ratio $\Delta = v(6\pi)/v(2\pi)$. Another important quantity is the *stroke volume* which is $v(6\pi)$. We can always increase this by scaling the compressor so we are really interested in the *normalized stroke volume* $\overline{V} = v(6\pi)/D^2$ where D is the diameter of the compressor. To simplify matters we use $|\mathbf{y}(10\pi) - \mathbf{y}(9\pi)|$ as an estimate of D. Finally we calculates the *leakage coefficient*:

$$l = \int_0^{2\pi} \sqrt{\kappa}\left(\frac{V_0}{V_1}\right)\left[\left(\frac{V_0}{V_1}\right)^\gamma - \left(\frac{V_1}{V_0}\right)^\gamma\right] dt,$$

see (71), where $\kappa(t) = \frac{1}{\rho_y(8\pi - t)} - \frac{1}{\rho_x(8\pi - t)}$, $V_0(t) = v(6\pi - t)$, $V_1(t) = v(4\pi - t)$, and $\gamma = 1.4$ as in section 7, page 28. The results are summarized in table 1 and in figure 10 we have drawn the three compressors.

	$s(\phi)$	R	d	Δ_1	Δ_2	Δ	$\overline{V}$	l
1	ϕ^2	4	2.28	1.43	1.75	2.49	0.085	0.64
2	$\phi^2 + \frac{1}{30}\phi^3$	6	2	1.68	2.14	3.60	0.041	0.67
3	$\phi^2 - \frac{1}{50}\phi^3 + \frac{1}{400}\phi^4$	6	2	2.25	2.76	6.21	0.016	1.13

Table 1: The performance of the three scroll compressors. The value $d = 2\pi - 4 \approx 2.28$ is the one which gives the circle involute scroll compressor constant wall thickness.

We should stress that example 2 and 3 are arbitrary and only are meant to illustrate that it is easy to calculate these important numbers. The calculation was done

using Maple® and except for the integration in the determination of l it is possible to get the result on symbolic form starting with a natural equation on polynomial form, say $s = c_0 + c_1\phi + c_2\phi^2 + c_3\phi^3 + c_4\phi^4$. We will not present the result of that calculation, but the possibility of doing this makes an optimization and a sensitivity analysis much easier.

If we compare the natural equation in example 2 and 3 with the natural equation $s = \phi^2$ for the circle involute it is clear that s is changed most for large values of ϕ corresponding to the outer part of compressor. It would be obvious to try to change the interior part of the compressor, because then the normalized stroke volume is kept fixed, while the volume ratio may change.

4 Leakage Between the Compression Chambers

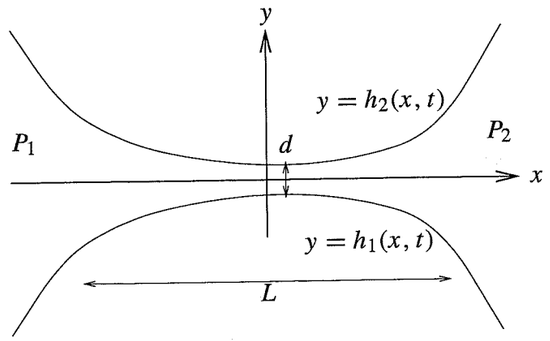

Figure 11: Schematic diagram of the gap between two chambers.

Ideally, the two halves of a scroll compressor remain perfectly in contact as they rotate. In reality it is not practical to machine them accurately enough for this to be the case, and instead there is a narrow gap. Typically the gap is around one micron across; this may be increased by wear and/or poor machining, and it is known that if it reaches around eight microns, the compressor becomes useless.

In this section we analyse the flow through this gap in an attempt to determine the leakage between neighbouring chambers in the compressor. We use compressible lubrication theory, using the fact that the gap has a very small aspect ratio. A schematic diagram of the geometry is given in figure 11. Here the gap, of typical thickness d and length L, separates two adjacent chambers containing gas at pressures P_1 and P_2. A local coordinate system is adopted with x pointing along the channel and y pointing across it. With respect to these coordinates we denote

Property	Symbol	Approx. value	Units
Viscosity	μ	10^{-5}	Pa s
Density	ρ	1	$\mathrm{Kg\,m^{-3}}$
Thermal diffusivity	k	2.5×10^{-2}	$\mathrm{J\,m^{-1}s^{-1}K^{-1}}$
Specific heat	c_v	10^3	$\mathrm{J\,Kg^{-1}K^{-1}}$
Gap thickness	d	10^{-6}	m
Contact length	L	10^{-2}	m
Rotation frequency	ω	50	$\mathrm{s^{-1}}$
Pressure drop	ΔP	10^6	Pa

Table 2: Estimated parameter values for leakage between cells in a scroll compressor.

the bottom and top of the channel (both of which are moving as the compressor rotates) by $y = h_1(x,t)$ and $y = h_2(x,t)$.

Some typical parameter values for the flow are shown in table 2. From these we can extract the important dimensionless parameters that determine the character of the flow. Firstly, the inverse aspect ratio of the channel is small,

$$\epsilon = \frac{d}{L} \approx 10^{-4}, \tag{35}$$

which will enable us to simplify the governing equations considerably. Next we deduce a typical velocity for the gas from a balance between the pressure drop and viscous drag:

$$U = \frac{d^2 \Delta P}{\mu L}.$$

Another dimensionless parameter is the ratio between this and the velocity due to rotation of the compressor:

$$\Omega = \frac{\omega L}{U} = \frac{\mu \omega L^2}{d^2 \Delta P} \approx 5 \times 10^{-2}. \tag{36}$$

Now we calculate the reduced Reynolds number using U as the velocity scale:

$$\mathrm{Re}^* = \frac{\rho U L \epsilon^2}{\mu} = \frac{\rho d^4 \Delta P}{\mu^2 L^2} \approx 10^{-4}. \tag{37}$$

Since Re^* is small, we can safely neglect inertia effects in the channel. We can also interpret Re^* as the square of a typical Mach number:

$$\mathrm{Re}^* = \frac{U^2}{c^2}, \quad \text{where } c^2 = \frac{\Delta P}{\rho},$$

and hence deduce that the flow is very much subsonic. Similarly, we calculate the reduced Peclet number using U as the velocity scale:

$$\mathrm{Pe}^* = \frac{\rho c_v U L \epsilon^2}{k} = \frac{\rho c_v d^4 \Delta P}{\mu k L^2} \approx 10^{-4}.$$

It is no accident that $\mathrm{Pe}^* \approx \mathrm{Re}^*$ since their ratio, the Prandtl number $\mathrm{Pr} = k/(\mu c_v)$, is approximately one for air.

We can immediately deduce a typical rate of leakage using the velocity scale U. The rate at which gas is lost through the channel is of order Ud, and so the cumulative loss over a cycle is typically Ud/ω. We simply have to compare this with the original area of a chamber to obtain the relative loss of gas due to leakage:

$$\text{relative loss} = \frac{d^3 \Delta P}{\mu \omega L^3} = \frac{\epsilon}{\Omega}. \tag{38}$$

The values given in table 2 suggest that this is rather small: about 0.2%. However, it is clearly highly sensitive to increases in d, and if we set $d = 8\ \mu$m, then the typical relative loss is dramatically increased to around 100%. This is in encouraging agreement with the experimental observations noted earlier.

4.1 Governing equations and boundary conditions

Our governing equations for the flow are the compressible Navier-Stokes equations (see [1])

$$\rho_t + \operatorname{div}(\rho \mathbf{u}) = 0, \tag{39}$$

$$\rho \frac{D\mathbf{u}}{Dt} = -\operatorname{grad} p + (\lambda + \mu)\operatorname{grad}\operatorname{div}\mathbf{u} + \mu \nabla^2 \mathbf{u}, \tag{40}$$

where $\mathbf{u}$ and p are the velocity and pressure fields, λ is the dilatational viscosity and D/Dt is the usual convective derivative. Coupled to these is the energy equation (see [1])

$$\rho c_v \frac{DT}{Dt} + p \operatorname{div}\mathbf{u} = k\nabla^2 T + \Phi, \tag{41}$$

where Φ is the dissipation,

$$\Phi = \lambda(\operatorname{div}\mathbf{u})^2 + \frac{\mu}{2}\left(\frac{\partial u_i}{\partial x_j} + \frac{\partial u_j}{\partial x_i}\right)^2. \tag{42}$$

Finally, the system is closed by specifying an equation of state. Treating the air as a perfect gas, we set

$$p = \rho R T, \tag{43}$$

where $R = c_p - c_v$ is the gas constant. It is convenient to substitute (39) and (43) into the left-hand side of (41) to obtain the energy equation in the form

$$\frac{1}{\gamma - 1}\frac{Dp}{Dt} - \frac{\gamma}{\gamma - 1}\frac{p}{\rho}\frac{D\rho}{Dt} = k\nabla^2 T + \Phi. \tag{44}$$

On the upper and lower boundaries of the channel we specify the velocity $\mathbf{u} = (u, v)$ of the gas to be the same as that of the channel wall:

$$u = u_i, \quad v = \frac{\partial h_i}{\partial t} + u_i \frac{\partial h_i}{\partial x}, \quad \text{on } y = h_i(x,t); \quad i = 1, 2. \tag{45}$$

Here the horizontal velocity u_i and position h_i of each wall are determined by the prescribed shape and motion of the scroll. We now integrate (39) with respect to y and apply the boundary conditions (45) to obtain an integrated equation representing total conservation of mass:

$$m_t + q_x = 0, \quad \text{where } m = \int_{h_1}^{h_2} \rho\, dy, \quad q = \int_{h_1}^{h_2} \rho u\, dy. \tag{46}$$

The quantities m and q represent respectively the mass density of fluid in, and flux of fluid through, each cross-section.

As boundary conditions for the temperature we assume that the channel walls are thermally insulated, so that

$$\frac{\partial T}{\partial y} = \frac{\partial h_i}{\partial x}\frac{\partial T}{\partial x} \text{ on } y = h_i(x,t); \quad i = 1, 2. \tag{47}$$

We also have to match the solution in the channel with the prescribed pressure in the chamber on either side:

$$p \to P_1 \text{ as } x \to -\infty, \quad p \to P_2 \text{ as } x \to +\infty. \tag{48}$$

4.2 Nondimensionalisation and leading-order equations

In nondimensionalising the equations (39–44) we utilize the slenderness of the geometry and the difference between the velocity scales for the fluid and for the

compressor. Thus we set

$$x = L\,x', \quad y = d\,y', \quad u = U u', \quad v = \epsilon U v', \quad t = \frac{t'}{\omega},$$
$$h_i = d\,h_i', \quad u_i = \omega L\,u_i', \quad p = \Delta P\,p', \quad \rho = \bar{\rho}\,\rho', \quad T = \frac{\Delta P\,T'}{\bar{\rho} c_v}. \tag{49}$$

Henceforth we drop the primes and proceed with the dimensionless variables. The Navier-Stokes equations (40), up to order Re* and ϵ^2, reduce to the *lubrication equations* (see [1])

$$p_y = 0, \quad u_{yy} = p_x. \tag{50}$$

Thus,

$$u = \frac{p_x}{2} y^2 + Ay + B, \tag{51}$$

where, using the dimensionless version of (45), A and B are found to be

$$A = \frac{\Omega(u_2 - u_1)}{h} - \frac{p_x(h_1 + h_2)}{2}, \quad B = \frac{\Omega(h_2 u_1 - h_1 u_2)}{h} + \frac{p_x h_1 h_2}{2}, \tag{52}$$

setting h to be the channel height:

$$h = h_2 - h_1.$$

Now consider the dimensionless version of the energy equation (44) and thermal boundary condition (47), taking only the terms at leading order in ϵ:

$$\frac{1}{\gamma - 1}\left(\Omega p_t + u p_x + v p_y\right) - \frac{\gamma}{\gamma - 1}\frac{p}{\rho}\left(\Omega \rho_t + u\rho_x + v\rho_y\right) - u_y^2 + O(\epsilon^2)$$
$$= \frac{1}{\mathrm{Pe}^*}\left(T_{yy} + O(\epsilon^2)\right), \tag{53}$$

$$T_y = O(\epsilon^2) \quad \text{on } y = h_1, h_2. \tag{54}$$

Now we use the fact that Pe* is much smaller than one to expand T as an asymptotic expansion in powers of Pe*:

$$T = T_0 + \mathrm{Pe}^* T_1 + \ldots.$$

Notice that, since $\epsilon^2 \ll \mathrm{Pe}^*$, it makes sense to keep terms of order Pe* while neglecting those of order ϵ^2.

To lowest order in Pe*, the Neumann problem (53, 54) simply tells us that

$$\frac{\partial T_0}{\partial y} = 0.$$

But from (50) we know that p is also independent of y to leading order, and thus ρ_y must likewise be zero. A relation between the as yet unknown functions $p(x,t)$ and $\rho(x,t)$ is obtained from the *solvability condition* for the inhomogeneous Neumann problem satisfied by T_1. The resulting equation is

$$\Omega p_t + \bar{u} p_x - \frac{\gamma p}{\rho}\left(\Omega \rho_t + \bar{u}\rho_x\right) = (\gamma - 1)\bar{u_y^2}, \tag{55}$$

where $\bar{\cdot}$ denotes the cross-sectional average:

$$\bar{\cdot} = \frac{1}{h}\int_{h_1}^{h_2} \cdot\, dy.$$

Now we simply substitute in the analytic form (51) of u to obtain

$$\Omega\left(p_t - \frac{\gamma p}{\rho}\rho_t\right) = \frac{\gamma h^2 p_x}{12}\left(p_x - \frac{p}{\rho}\rho_x\right). \tag{56}$$

A second equation linking p and ρ is obtained by substituting (51) into the dimensionless form of (46), the result of which is

$$\Omega(\rho h)_t + q_x = 0, \quad \text{where } q = \frac{\Omega\rho h(u_1 + u_2)}{2} - \frac{\rho p_x h^3}{12}. \tag{57}$$

4.3 Solution in the quasi-steady limit

Equations (56) and (57) form a closed leading-order system for ρ and p; recall that u_1, u_2 and h are prescribed functions of x and t. They can be simplified further by taking the *quasi-steady limit* $\Omega \to 0$. Then, from (56) we deduce that

$$\frac{\partial}{\partial x}\left(\frac{p}{\rho}\right) = 0, \tag{58}$$

which implies that the gas is *isothermal*. So in (57) we can set $\rho = p/(T(\gamma - 1))$ where T is constant. Thus the flux

$$q = -\frac{h^3 p p_x}{12T(\gamma - 1)} \tag{59}$$

is a function only of t. Now we simply divide by h^3 and integrate with respect to x from $-\infty$ to $+\infty$, applying the matching conditions (48), to obtain

$$q = \frac{p_1^2 - p_2^2}{24T(\gamma - 1)} \left(\int_{-\infty}^{\infty} \frac{dx}{h^3} \right)^{-1}. \tag{60}$$

This tells us the flux, *i.e.* the leakage, through the channel, and how it depends on the pressure in the chamber on either side and the geometry of the channel.

Since the minimum gap thickness is very small, the integral in (60) is dominated by the behaviour of h near its minimum. In a neighbourhood of this point, we can approximate h by a quadratic function (which in general it will be locally) say

$$h = d(t) + \frac{\kappa(t)x^2}{2},$$

where κ is the *difference between the curvatures* of the two channel walls at their closest point. Then

$$\int_{-\infty}^{\infty} \frac{dx}{h^3} = \frac{3\pi}{4d^{5/2}\sqrt{2\kappa}}.$$

5 Conservation Equations for the Chambers

Now we consider the conservation of mass and energy for a single chamber of gas. Since the Reynolds number on the scale of a chamber is large, it is common practice to assume that the gas in each chamber is turbulent and thus well-mixed. Hence we can associate a spatially-uniform temperature $T(t)$ and pressure $P(t)$ with the mass $M(t)$ of gas in the chamber, which has a given volume $V(t)$.

Firstly, note that the ratio of kinetic to thermal energy is of order

$$\frac{\text{kinetic energy}}{\text{thermal energy}} \sim \frac{\bar{\rho}\omega^2 L^2}{\Delta P} = \Omega^2 \mathrm{Re}^* \ll 1.$$

Therefore we neglect kinetic energy throughout, so that the internal energy in the chamber is simply

$$E = Mc_v T. \tag{61}$$

The internal energy is changed due to:

- The work done by changes in the volume V of the chamber which, recall, is assumed to be a prescribed function of time. The work done is given by $-P\,dV/dt$.

- The energy transported into and out of the chamber through the gaps on either side. Assuming the flow through these gaps is adiabatic, the energy transported by a mass flux q is qH, where H is the *enthalpy*, equal to $c_p T$.

- Dissipation and energy losses to the external environment, which we denote by $\dot{Q}$.

Putting all these together, we obtain

$$\frac{dE}{dt} = -P\frac{dV}{dt} + q_i c_p T_i - q_o c_p T + \dot{Q}, \tag{62}$$

where the subscripts i and o correspond to flow into and out of the chamber respectively. Notice that the temperature of gas flowing out of the chamber is the same as that of the gas in the chamber, T.

Henceforth we neglect $\dot{Q}$, although thermal interaction with the surroundings might be included in a more refined model. Therefore, substituting (61) into (62) and rearranging, we obtain an ordinary differential equation relating P and T:

$$V\frac{dP}{dt} = \gamma R(q_i T_i - q_o T) - \gamma P\frac{dV}{dt}. \tag{63}$$

Next we consider conservation of mass for the chamber. This simply states that the mass change is equal to the flux into the chamber minus that out:

$$\frac{dM}{dt} = q_i - q_o. \tag{64}$$

But $M = \rho V$, where the density ρ is given in terms of P and T by using the equation of state (43). Thus (64) can be rearranged to a second equation relating P and T:

$$\frac{dT}{dt} = \frac{T}{P}\frac{dP}{dt} + \frac{T}{V}\frac{dV}{dt} - \frac{RT^2}{PV}(q_i - q_0). \tag{65}$$

Now the idea is as follows. Given the pressure P and temperature T in two neighbouring chambers, and the geometry of the gap between them, we can evaluate the flux from one to the other using (60). Then for each chamber we have the two differential equations (63, 65) for P and T, which are coupled to the corresponding equations for the neighbouring chambers by the fluxes q on either side.

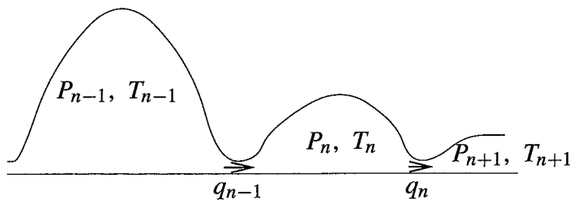

Figure 12: Schematic diagram of the coupling between neighbouring chambers.

6 The Coupled Problem

The situation is depicted schematically in figure 12. We have a series of chambers, in the n^{th} of which the gas is at pressure P_n and temperature T_n. The flux between the n^{th} and $(n+1)^{\text{th}}$ chamber is denoted by q_n, with the sign convention that $q_n > 0$ if gas flows *from* chamber n *to* chamber $(n+1)$.

From the theory of section 4, we know that in each of the gaps between the chambers the temperature is constant, but the value of that constant is determined by the sign of q: if $q_n > 0$ then the gas transported by q_n has temperature T_n, while if $q_n < 0$ it is at T_{n+1}. Thus, when we redimensionalise (60) we obtain the following expression for q_n:

$$q_n = \frac{\left(P_n^2 - P_{n+1}^2\right) d^{5/2}\sqrt{\kappa}}{9\pi\sqrt{2}\,\mu R} \begin{cases} 1/T_n & \text{if } P_n > P_{n+1}, \\ 1/T_{n+1} & \text{if } P_n < P_{n+1}. \end{cases} \tag{66}$$

Similarly, when we write down the conservation equations (63, 65) for the n^{th} chamber, whether each of q_{n-1} and q_n qualifies as flux *into* (q_i) or *out of* (q_o) the chamber depends on its sign. The resulting equations can conveniently be written in the form

$$\frac{\dot{P}_n}{P_n} = \frac{\gamma R}{P_n V_n}\left\{q_{n-1}T_n - q_n T_{n+1} + q_{n-1}^+(T_{n-1} - T_n) + q_n^+(T_{n+1} - T_n)\right\} - \frac{\gamma \dot{V}_n}{V_n}, \tag{67}$$

$$\frac{\dot{T}_n}{T_n} = -\frac{(\gamma-1)\dot{V}_n}{V_n} + \frac{R}{P_n V_n}\left\{q_n T_n - \gamma q_n T_{n+1} + (\gamma-1)q_{n-1}T_n + \gamma q_{n-1}^+(T_{n-1} - T_n) + \gamma q_n^+(T_{n+1} - T_n)\right\}, \tag{68}$$

where q^+ denotes the positive part of q:

$$q^+ = \begin{cases} q & \text{if } q > 0, \\ 0 & \text{if } q < 0. \end{cases}$$

To solve the dynamical system (67, 68) we need to apply "end conditions" at the outermost chambers. Suppose there are N chambers altogether, with the first and N^{th} open to reservoirs at *given* pressure and temperature P_0, P_N and T_0, T_N. Note that T_0 and/or T_N need only be specified if $P_0 > P_1$ and/or $P_N > P_{N-1}$, so that gas flows *into* the adjoining chambers. We also have to specify P_n and T_n for $n = 1, \ldots, N-1$ at $t = 0$. Finally, there is a complicated closure condition associated with the periodicity of the motion. Roughly speaking, it is clear that after a complete cycle, what was the n^{th} chamber has now become the $(n+1)^{\text{th}}$ chamber. The way in which this condition is implemented in practice should be made clear by the following outlined solution procedure.

1. Suppose P_n and T_n are given at $t = 0$ for $n = 1, \ldots, N$.
2. Integrate the coupled ordinary differential equations (67, 68) forward through one complete cycle, using the specified values of P_0, T_0, P_N, T_N.
3. Set
$$\begin{pmatrix} V_n \\ P_n \\ T_n \end{pmatrix}_{\text{new}} = \begin{pmatrix} V_{n-1} \\ P_{n-1} \\ T_{n-1} \end{pmatrix}_{\text{old}}.$$
4. Go to step 2.

The desired final result is a periodic solution, in which the "new" and "old" values in step 3 above are identical, that is

$$\text{periodic solution} \;\Rightarrow\; \begin{pmatrix} V_n(t) \\ P_n(t) \\ T_n(t) \end{pmatrix} \equiv \begin{pmatrix} V_{n-1}(t+\tau) \\ P_{n-1}(t+\tau) \\ T_{n-1}(t+\tau) \end{pmatrix},$$

where $\tau = 2\pi/\omega$ is the period of the motion. However, when there is strong coupling between the chambers it is far from clear that this periodic solution is unique or stable. Indeed, for a high-dimensional nonlinear dynamical system such as this, we might expect to see extremely complicated dynamics in general.

6.1 The small coupling limit

If the leakage is relatively small (which it should be for any worthwhile compressor), we can perturb about the zero-q solution (in which mass and entropy are preserved in each chamber)

$$P_n = P_0\left(\frac{V_0}{V_n}\right)^{\gamma}, \quad T_n = T_0\left(\frac{V_0}{V_n}\right)^{\gamma-1}. \tag{69}$$

Then the lowest-order fluxes are obtained by substituting (69) into the expression (66) for q_n.

Interestingly, if the compressor is in a periodic state, we only need to find q_0 to evaluate the total leakage: in its first cycle, a chamber *gains* $-q_1$ and loses $-q_0$. Then, in the next cycle, it *loses* $-q_1$ and gains $-q_2$. Over the lifetime of a chamber, all the intermediate fluxes cancel each other out, so only q_0 remains. In the small-q limit, this is readily evaluated:

$$-q_0 = \frac{P_0^2 d^{5/2}\sqrt{\kappa}}{9\pi\sqrt{2}\,\mu R T_0}\left(\frac{V_0}{V_1}\right)\left[\left(\frac{V_0}{V_1}\right)^\gamma - \left(\frac{V_1}{V_0}\right)^\gamma\right]. \tag{70}$$

Thus, assuming that d and the other parameters in (70) are constant (and beyond our control), we obtain a functional form of the total leakage:

$$\text{total leakage} \propto l := \int_0^\tau \sqrt{\kappa}\left(\frac{V_0}{V_1}\right)\left[\left(\frac{V_0}{V_1}\right)^\gamma - \left(\frac{V_1}{V_0}\right)^\gamma\right] dt. \tag{71}$$

We can use this functional as part of a cost function in evaluating proposed new compressor designs, for all the variables on the right-hand side of (71) can readily be evaluated for any given scroll geometry. Without performing any detailed calculations, we can immediately deduce some desirable design properties that will reduce leakage:

- The contact should be as *flat* as possible, *i.e.* κ should be minimised.
- The volume should be *reduced gradually on the first cycle*. This follows from the observation that only q_0 is relevant to the total mass loss.

7 Numerical Results

In this section we present some preliminary numerical simulations of the system (67, 68). We consider the simple configuration shown schematically in figure 13. Here, at the beginning of the cycle (diagram 1) the shaded volume of gas V_1 is taken in from the atmosphere. As V_1 decreases (diagram 2) the gas is compressed until the cycle is completed (diagram 3). Then the gas is released into a reservoir of constant volume V_2 (diagram 4). The idea is that we run the simulation through several such cycles and see what pressure we can achieve in the reservoir; this seems like a good measure of the efficacy of the compressor.

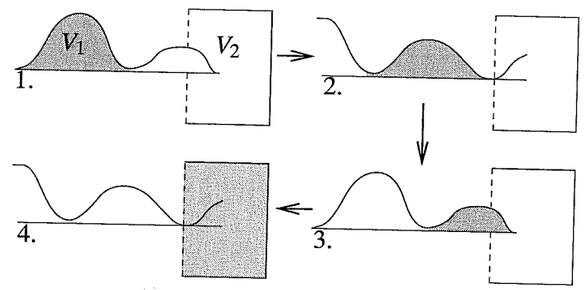

Figure 13: Schematic diagram of the compression of a single chamber (of volume V_1) which opens up into a reservoir of volume V_2.

The coupled system for the temperature and pressure in the two chambers is

$$\frac{\dot P_1}{P_1} = \frac{\gamma R}{P_1 V_1}\{q_0 T_1 + (T_0 - T_1) q_0 H(P_0 - P_1) - q_1 T_2 + (T_2 - T_1) q_1 H(P_1 - P_2)\} - \frac{\gamma \dot V_1}{V_1}, \tag{72}$$

$$\frac{\dot T_1}{T_1} = -\frac{(\gamma-1)\dot V_1}{V_1} + \frac{R}{P_1 V_1}\{q_1 T_1 - \gamma q_1 T_2 + (\gamma-1) q_0 T_1 + \gamma(T_0 - T_1) q_0 H(P_0 - P_1) + \gamma(T_2 - T_1) q_1 H(P_1 - P_2)\}, \tag{73}$$

$$\frac{\dot P_2}{P_2} = \frac{\gamma R}{P_2 V_2}\{q_1 T_2 + (T_1 - T_2) q_1 H(P_1 - P_2)\}, \tag{74}$$

$$\frac{\dot T_2}{T_2} = \frac{R}{P_2 V_2}\{(\gamma-1) q_1 T_2 + \gamma(T_1 - T_2) q_1 H(P_1 - P_2)\}, \tag{75}$$

where H is the Heaviside function and

$$\begin{aligned} q_0 &= \frac{d^{5/2}\sqrt{\kappa}}{9\pi\sqrt{2}\,\mu R}(P_0^2 - P_1^2)\left\{\frac{1}{T_1} + \left(\frac{1}{T_0} - \frac{1}{T_1}\right) H(P_0 - P_1)\right\} \\ q_1 &= \frac{d^{5/2}\sqrt{\kappa}}{9\pi\sqrt{2}\,\mu R}(P_1^2 - P_2^2)\left\{\frac{1}{T_2} + \left(\frac{1}{T_1} - \frac{1}{T_2}\right) H(P_1 - P_2)\right\}. \end{aligned} \tag{76}$$

With the ambient temperature T_0 and pressure P_0 given and specified chamber volume $V_1(t)$ and (constant) reservoir volume V_2, (72–76) is a well-defined problem for $\{P_1, P_2, T_1, T_2\}$. We initiate the calculations with $P_1 = P_2 = P_0$, $T_1 = T_2 = T_0$.

As outlined in section 6 at the end of each cycle we perform a replacement algorithm corresponding to (*i*) a new chamber of atmospheric gas forming in the "new" V_1; (*ii*) the "old" V_1 discharging into V_2. For the latter we find the new values of P_2 and T_2 by setting the mass and energy in V_2 after the discharge equal to the total mass and energy in V_1 and V_2 immediately prior to the discharge. Thus, after the n^{th} cycle we set

$$\begin{aligned} P_1(n\tau+) &= P_0, \\ T_1(n\tau+) &= T_0, \\ P_2(n\tau+) &= \left[\frac{P_1V_1 + P_2V_2}{V_1 + V_2}\right](n\tau-), \\ T_2(n\tau+) &= \left[\frac{(P_1V_1 + P_2V_2)T_1T_2}{P_1V_1T_1 + P_2V_2T_2}\right](n\tau-). \end{aligned} \tag{77}$$

In all the calculations to follow the parameter values are set as follows,

$$\begin{aligned} \mu &= 1, & R &= 1, & \gamma &= 1.4, & \kappa &= 1, \\ P_0 &= 1, & T_0 &= 1, & V_2 &= 10, & \tau &= 1, \end{aligned}$$

and we examine the effects of varying the "leakage parameter" d and the form of $V_1(t)$. We start with the simplest case in which V_1 is linear in t, say

$$V_1 = 1 - \alpha t,$$

where $\alpha \in (0, 1)$; $\alpha = 0$ implies a compression ratio of one, while as $\alpha \to 1$ the compression ratio goes to infinity. In figure 14 we plot the pressure in the chamber and the reservoir versus time for the case $\alpha = 0.5$, $d = 1$. We can see how P_1 increases during each cycle and is reset each time a new cycle begins. In the reservoir, P_2 varies only slightly during any cycle, and is incremented gradually at each discharge. Closer examination reveals that, because of leakage between the chamber and the reservoir, P_2 *decreases* when $P_2 > P_1$ and *increases* when $P_2 < P_1$. For these parameter values, the system appears to settle down to a periodic state after around 60 cycles, with the pressure in the reservoir enhanced by a factor of just over 2.

In figure 15 we show the corresponding behaviour of the temperature for the same parameter values. The behaviour is seen to be rather similar to that of the pressure. Henceforth we do not bother to present the results for the temperature since it is irrelevant to the total stored energy, which is proportional to P_2V_2.

In figure 16 we present the results for the pressure variations when $\alpha = 0.8$, so the compression ratio is five, compared with two in the previous calculations. As

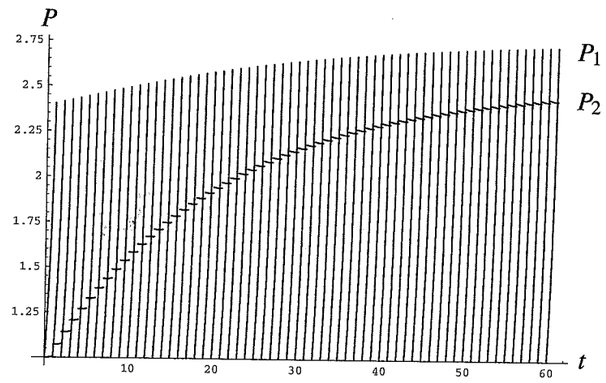

Figure 14: Pressures P_1 (in the compression chamber) and P_2 (in the pressurised reservoir) versus time. The volumes are $V_1 = 1 - 0.5\,t$, $V_2 = 10$ and the leakage parameter $d = 1$.

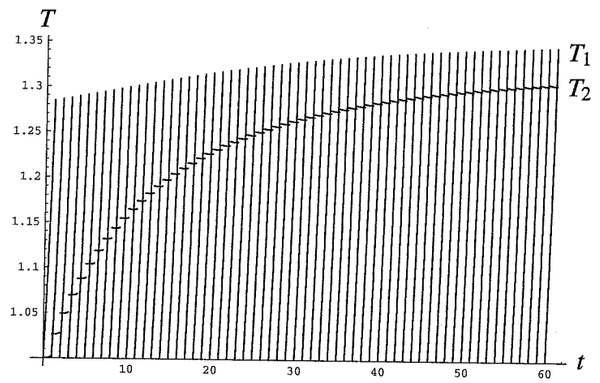

Figure 15: Temperatures T_1 (in the compression chamber) and T_2 (in the pressurised reservoir) versus time. The volumes are $V_1 = 1 - 0.5\,t$, $V_2 = 10$ and the leakage parameter $d = 1$.

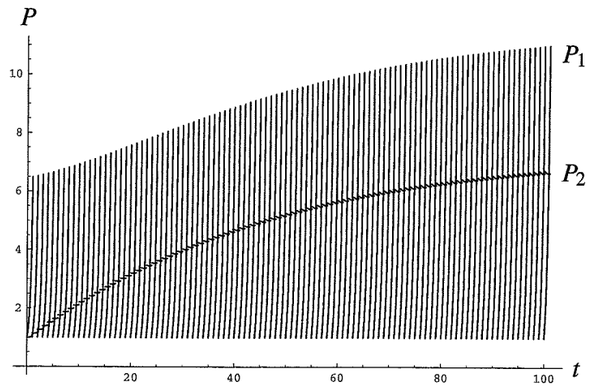

Figure 16: Pressures P_1 (in the compression chamber) and P_2 (in the pressurised reservoir) versus time. The volumes are $V_1 = 1 - 0.8\,t$, $V_2 = 10$ and the leakage parameter $d = 1$.

expected, the increased compression ratio leads to a somewhat higher final pressure, although the system also takes somewhat longer to converge to its periodic state.

In the light of figures 14 and 16 it is of interest to ask how the final pressure achieved in the reservoir depends on the compression ratio, *i.e.* on α. As a measure of this we take the average of P_2 over the 100^{th} cycle:

$$\bar{P}(100) = \int_{100}^{101} P_2\,dt,$$

and plot the result versus α for various values of d in figure 17. Not surprisingly the pressure achieved increases as α is increased and as d is decreased. However, for sufficiently small d, decreasing d still further doesn't appear to have much effect; the graphs for $d = 0.25$ and $d = 0.5$ are virtually indistinguishable. This is explained by examination of the transients, which makes it clear that for these small values of d, P_2 has yet to equilibrate after 100 cycles.

So, we have shown the rather obvious results that the effectiveness of a compressor can be enhanced by increasing the compression ratio and by minimising the leakage, although these also make the convergence to maximum compression slower. Next we would like to compare compressors with the same compression ratio but different histories $V_1(t)$. Therefore we consider the family

$$V_1 = 1 - \beta t + (V_f + \beta - 1)t^2,$$

shown in figure 18, where V_f is the final volume (so the volume ratio is $1/V_f$) and β changes the volume history for a fixed V_f; $\beta = 1 - V_f$ gives the linear

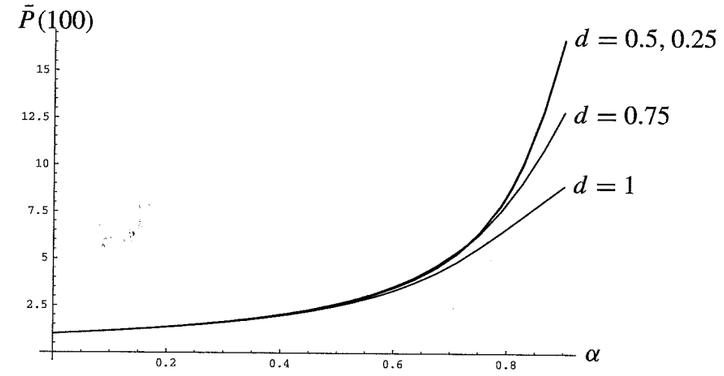

Figure 17: Average reservoir pressure over the 100^{th} cycle versus compression parameter α. The volumes are $V_1 = 1 - \alpha t$, $V_2 = 10$ and the leakage parameter $d = 0.25, 0.5, 0.75, 1$. Notice that the curves for $d = 0.25$ and $d = 0.5$ are indistinguishable.

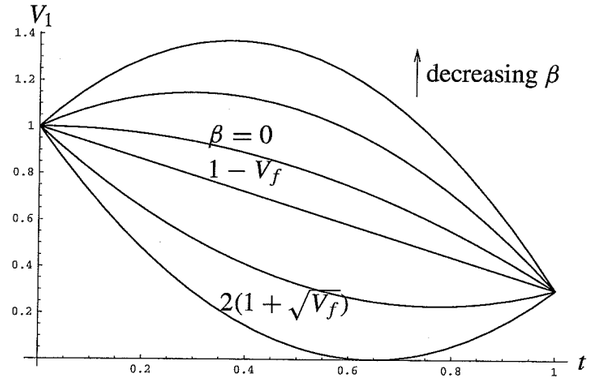

Figure 18: The family of curves $V_1 = 1 - \beta t + (V_f + \beta - 1)t^2$ for various values of β (here $V_f = 0.3$). The value $\beta = 1 - V_f$ gives a straight line joining $V_1 = 1$ at $t = 0$ to $V_1 = V_f$ at $t = 1$; $\beta = 0$ has zero gradient at $t = 0$; $\beta = 2(1 + \sqrt{V_f})$ is the value at which V_1 first reaches zero for $t \in (0, 1)$.

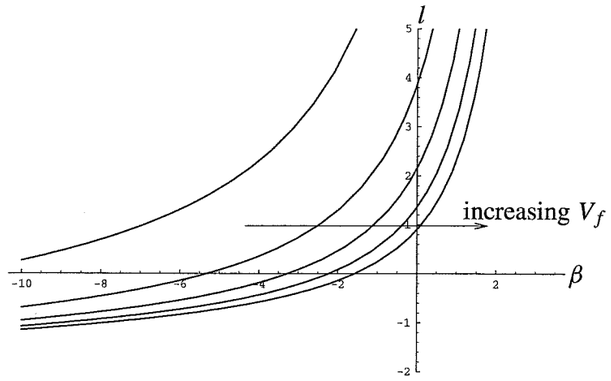

Figure 19: Theoretically predicted leakage $l = \int_0^1 (V_1^{-\gamma-1} - V_1^{\gamma-1})\,dt$ for the family of volume histories depicted in figure 18; $V_1 = 1 - \beta t + (V_f + \beta - 1)t^2$ with $V_f = 0.1, 0.2, 0.3, 0.4, 0.5$.

$V_1(t)$, *i.e.* constant compression rate, considered previously. Broadly speaking, if β is decreased the compression is slower initially and accelerates towards the end of the cycle, and vice versa.

Firstly we check how our theoretical approximate leakage l given in (71) varies with β. In figure 19 we plot l versus β for different values of V_f. We observe that the theoretical leakage for a given volume ratio is reduced if the compression is slow at the beginning and faster at the end. This echoes the suggestion at the end of section 6 that the volume should be reduced gradually at the start. There is a surprise, however, in that l can be *negative* if β is sufficiently large and negative. This corresponds to large positive excursions in V_1 (see figure 18), as a result of which the compressor acts like a bellows, sucking extra gas into the chamber.

This conclusion is backed up by figure 20 in which we plot $\bar{P}(100)$ from our simulation versus β for different values of V_f (and with $d = 1$). Here the behaviour in general is extremely interesting; depending on the volume ratio $\bar{P}$ may be an increasing or decreasing function of β, or may vary nonmonotonically. However, for the large volume ratios which are likely to be of most practical interest, the optimal performance (*i.e.* largest possible value of $\bar{P}(100)$) is obtained by making β as large and negative as possible.

8 Conclusions

We have used the natural equation of a curve to define the geometry of the scrolls, and this allows us to obtain all the geometric properties of scroll compressor on

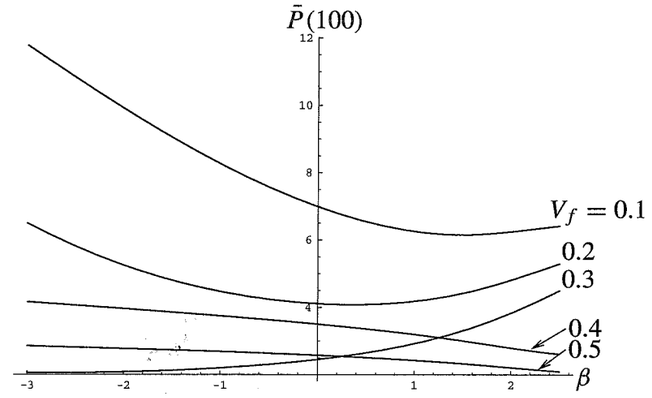

Figure 20: Average reservoir pressure over the 100th cycle for $d = 1$ and the family of volume histories depicted in figure 18; $V_1 = 1 - \beta t + (V_f + \beta - 1)t^2$ with $V_f = 0.1, 0.2, 0.3, 0.4, 0.5$.

symbolic form if we give the arc length as a polynomial in the tangent direction. The formulas are especially simple if we restrict ourself to compressors with a circular orbit.

We have characterized all compressors with a circular orbit and constant wall thickness, and have argued that these compressors do not offer any advantages over the standard circle involute compressor.

We have outlined a procedure which design a compressor given the natural equation of one of the sides, the radius of the circular motion, and the thickness of the scroll wall at one place. That compressor has the property that the two scrolls are the same just rotated 180° degrees relative to each other.

There is no guarantee that the scroll compressors constructed this way are physical realizable, basicly the radius of the circular motion and the thickness of the walls should be sufficiently small. It would be possible to give estimates on the bounds for these two numbers, but this has not been investigated.

We have used compressible lubrication theory to obtain a theoretical prediction of the leakage between adjoining chambers in a scroll compressor. One surprising outcome of the analysis is that the gas flowing through the narrow gap between one chamber and the next is *isothermal*. In traditional inviscid gas dynamics one would expect the temperature to decrease as the gas accelerates through the gap, while classical lubrication theory would predict an increase in temperature due to viscous dissipation. Remarkably these two effects appear to cancel each other out exactly.

Our result for inter-chamber leakage was then incorporated in a coupled model for the pressure and temperature of the gas in each chamber. The model takes the form of a dynamical system, whose general properties certainly warrant further investigation. Our analysis was limited to examination of the case in which the leakage is small. In this limit we obtained an approximate measure of the total losses due to leakage, as a functional of the geometry of the compressor. This could in future be included in a cost function for evaluating proposed new compressor designs.

We performed some numerical simulations of a simple compressor with just one chamber pumping gas into a sealed reservoir. From these we were able to test the effects on compressor performance of varying the leakage rate, the volume ratio and the volume history. The most intriguing possibility suggested by the simulations is that of making the chamber volume *increase* initially, before a rapid compression just prior to discharge. This allows the compressor to use the leakage in its favour by sucking more gas in from the atmosphere.

Many potentially important physical effects have been neglected in this study, and might be considered in the future to refine the model further. These include thermal losses through the compressor walls, and the "squeeze film" and "Couette" effects in the lubrication analysis (*i.e.* the terms multiplied by Ω in (56, 57)). Perhaps most importantly, we have restricted our analysis to a two-dimensional configuration, and thus have not considered leakage through the sides of the chambers. The results of section 4 should be applicable to these regions also.

Finally we have demonstrated how to combine the geometry and the leakage analysis to estimate the leakage of a compressor with a given geometry.

Acknowledgement

We thank DANFOSS and in particular Stig Helmer Jørgensen for providing us with an interesting problem and answering many question during the week.

Bibliography

[1] Ockendon, H. & Ockendon, J. R., *Viscous Flow*, Cambridge University Press, Cambridge, 1995.

The Group Working on the Problem

Jens Gravesen, [J.Gravesen@mat.dtu.dk]
Vagn Lundsgaard Hansen, [V.L.Hansen@mat.dtu.dk]
Christian Henriksen, [Christian.Henriksen@mat.dtu.dk]
Peter Howell, [howell@math.ox.ac.uk]
Stig Helmer Jørgensen, [SHJ@danfoss.com]
John W. Perram, [jperram@mip.ou.dk]